Thermodynamic fluctuations between magnetic states from first-principles phonon calculations: The case of bcc Fe

Shun-Li Shang,* Yi Wang, and Zi-Kui Liu
Department of Materials Science and Engineering, The Pennsylvania State University, University Park, Pennsylvania 16802, USA
(Received 5 August 2009; revised manuscript received 26 April 2010; published 23 July 2010)

The longstanding issue of magnetic thermodynamics containing anomalies can be resolved using a reliable model at finite temperatures: thermodynamic fluctuations among the competing collinear magnetic configurations (especially the low energy ones) in accordance with canonical partition function. Based on first-principles phonon calculations, we shed light on the magnetic materials (as exemplified in bcc Fe): the Schottky anomaly of heat capacity and the pressure-dependent Curie temperature stem from the magnetic configurational entropy due to the competition of various magnetic states.

DOI: 10.1103/PhysRevB.82.014425 PACS number(s): 75.40.Cx, 63.20.−e, 64.70.qd, 71.15.Mb

I. INTRODUCTION

Great success of first-principles thermodynamics at finite temperatures has been achieved in solid states with the Helmholtz free energy of a state/phase σ given by[1–4]

$$F^{\sigma}(V,T) = E_0^{\sigma}(V) + F_{vib}^{\sigma}(V,T) + F_{ele}^{\sigma}(V,T), \tag{1}$$

where V is the volume, T the temperature, E_0^{σ} the static energy at 0 K obtained from first-principles directly, F_{vib}^{σ} the vibrational contribution estimated by, e.g., first-principles phonon calculations,[2] and F_{ele}^{σ} the thermal electronic contribution determined via integration over the electronic density of state following the Fermi-Dirac distribution.[1] However, little can be said for sure about the thermodynamics in magnetic materials due to the occurrence of phase transition at the Curie (or Néel) temperature. For example the widely adopted treatment of magnetic contribution to Helmholtz energy [see Eq. (1)] is to add an extra magnetic term $F_{mag}^{\sigma}(V,T)$ based on the Heisenberg model in mean-field or random-phase approximation.[5] According to this scheme, Körmann *et al.*[5] predicted well the first-principles heat capacity of bcc Fe below the Curie temperature, but the experimental data[6] above the Curie temperature cannot be depicted even with considering the contribution of magnon energy, indicating the faultiness of the Heisenberg model. Another example is that the treatment of disordered magnetic phase using the special quasirandom structure (SQS) method[7] employs only one special magnetic state (see the application in paramagnetic CrN phase[8]), implying its inability to describe the anomalous magnetic phenomena. In addition, Hobbs *et al.*[9] indicated that the energy difference between the collinear magnetic structure of α-Mn and the noncollinear one of α-Mn is negligibly small (almost equal), implying that we cannot use this energy difference to predict the Néel temperature of α-Mn using, e.g., the mean-field model.

According to our knowledge, the existing treatments of magnetic contribution (e.g., the aforementioned examples) all fail (or possess problems) to probe the longstanding issues of magnetic materials, such as the nature of Curie/Néel temperature and the Schottky anomaly of heat capacity. A reliable thermodynamic model at finite temperatures is therefore needed for magnetic materials and motivates the present work. The magnetic thermodynamics of bcc Fe will be investigated herein in order to demonstrate our approach as shown below. The selection of Fe is due to its great importance for practical applications (e.g., steel) and its abundance in earth's core. In particular the success of Fe will open an avenue to explore the intriguing properties of magnetic materials, such as, multiferroics,[10] lithium transition metal phosphates for rechargeable batteries,[11] Invar alloys, heavy fermion,[12] and iron-based superconductors.[13,14]

II. THEORY AND METHODOLOGY

A. Magnetic thermodynamics

The present work aims to propose an alternative first-principles thermodynamic approach for magnetic materials with demonstration in bcc Fe. To this end, we assume that (i) magnetic material at finite temperatures can be described by a mixture of many collinear magnetic (micro)states competing with each other, i.e., by mixing of the spin-flipping configurations (SFCs), and (ii) the SFC system belongs to canonical ensemble under the constant NVT framework (N: number of particles, V: volume, and T: temperature) described by the canonical partition function,

$$Z = \sum_{\sigma} Z^{\sigma} = \sum_{\sigma} w^{\sigma} \exp(-\beta F^{\sigma}), \tag{2}$$

where $\beta = 1/(k_B T)$ with k_B being the Boltzmann's constant, w^{σ} the degeneracy factor (multiplicity) of state σ, and F^{σ} the Helmholtz energy of σ at V and T. According to Eq. (2), the total Helmholtz energy of the SFC system can be written by[15]

$$F = -\log(Z)/\beta = \sum_{\sigma} x^{\sigma} F^{\sigma} - TS_{conf}, \tag{3}$$

where $x^{\sigma} = Z^{\sigma}/Z$ is the thermal population (probability) of σ including the w^{σ}, i.e., $Z^{\sigma} = w^{\sigma} \exp(-\beta F^{\sigma})$ [see Eq. (2)]. S_{conf} is the magnetic configurational entropy introduced automatically by partition function,[15]

$$S_{conf} = -k_B \sum_{\sigma} [x^{\sigma} \log(x^{\sigma}) - x^{\sigma} \log(w^{\sigma})], \tag{4}$$

where the first term containing $x^{\sigma} \log(x^{\sigma})$ is the mixing configurational entropy due to different magnetic states, the sec-

ond term containing $x^\sigma \log(w^\sigma)$ is the degeneracy configurational entropy. E.g., for ferromagnetic configuration (FMC) with $w=2$ (spin-up and spin-down) and $x=1$, the degeneracy configurational entropy has the known value of $k_B \log 2$ due to the freedom of spin.[16] When more configurations (i.e., SFCs) are considered in a magnetic ensemble, the magnetic configurational entropy, including both the mixing configurational entropy and the degeneracy configurational entropy, will be introduced by partition function, and the addition of extra magnetic term to Helmholtz energy (e.g., in Heisenberg model) is therefore not needed. Note that it is the magnetic configurational entropy S_{conf} that makes the Helmholtz energies of some of the 0 K metastable states lower than the original 0 K ground state at elevated temperatures, resulting in the magnetic phase transition. Hence, the introduction of S_{conf} will be a key to probe the anomalies in magnetic materials. Based on Eq. (3), all the other thermodynamic functions can be deduced, e.g., the heat capacity at constant volume,

$$C_V = \sum_\sigma x^\sigma C_V^\sigma + C_V^m = \sum_\sigma x^\sigma C_V^\sigma + (\beta/T)\left[\sum_\sigma x^\sigma (E^\sigma)^2 - \left(\sum_\sigma x^\sigma E^\sigma\right)^2\right], \quad (5)$$

where C_V^σ is the heat capacity at constant volume of state σ, C_V^m the magnetic heat capacity at constant volume due to S_{conf}, and E^σ the internal energy of σ at V and T ($E^\sigma = F^\sigma + TS^\sigma$). As shown below, the introduction of C_V^m arising from the competition among magnetic states will result in a heat capacity bump, i.e., the Schottky anomaly.

In principle, our model is an improved one based on the Ising-type description with two major improvements. The first one is the introduction of V- and T-dependent F^σ in the partition function of Eq. (2). In previous applications, the 0 K static energy of state σ was usually employed in the partition function, see such as Refs. 17 and 18. The second improvement is that we point out the configurational entropy introduced by partition function accounts for the anomalies of magnetic materials, depicting well the short range interactions (among collinear magnetic microstates). According to the calculated F^σ from quasiharmonic approach [see Eq. (1)], both Z^σ and Z can be obtained [see Eq. (2)], and in turn, x^σ and S_{conf} are resulted [see Eqs. (3) and (4)]. Therefore, we propose an alternative approach to determine x^σ and S_{conf} from first-principles phonon calculations.

B. Magnetic ensemble of bcc Fe

Regarding the *practice* of our model, we found the collinear magnetic configurations (ignoring the noncollinear, magnon, and spin-wave cases, etc.) work well for magnetic thermodynamics. Other successful applications using collinear magnetic configurations include, e.g., (i) the mean-field model applying the magnetic exchange energy caused by the exchange of spin-up and spin-down atoms and (ii) the disordered spin-up and spin-down magnetic moments in paramagnetic CrN phase[8] mimicked by SQS method.[7] For the sake of simplicity, in the present work the canonical ensemble of magnetic (micro)states with collinear spin alignments is restricted in a 16-atom $1\times1\times8$ supercell of bcc Fe, resulting in 65 536 spin-flipping configurations (SFCs). Calculations demonstrate that the non-neighboring spin up (or spin down) alignments are numerically unstable (or possess imaginary phonon modes). Convergence to neighboring spin up (down) states always occurs. Our tests based on cluster expansion method (CEM,[19–21] see Appendix for details) show that the unstable states are high in energy and hence can be neglected according to the Boltzmann distribution [see also our partition function of Eq. (2)]. The remaining 12 stable (str1, i.e., FMC) and metastable states (str2 to str12) are sketched in Fig. 1 with the degeneracy factors of 2, 32, 32, 32, 32, 32, 32, 16, 16, 16, 8, and 4, respectively, totaling 254 configurations. For the convenience of discussion, the mentioned SFCs hereafter exclude the FMC (str1).

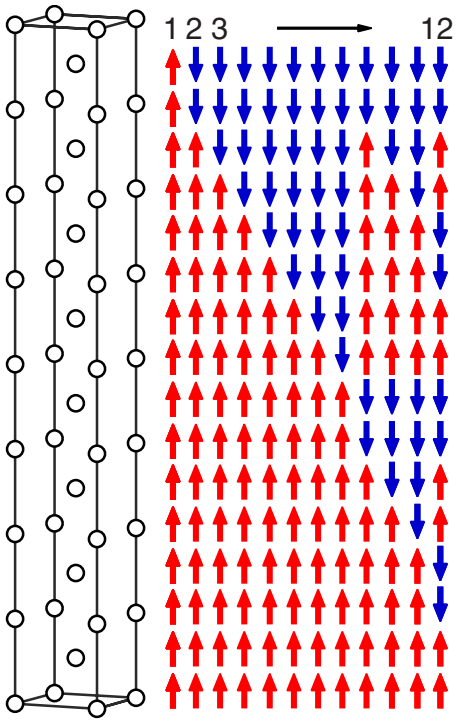

FIG. 1. (Color online) $1\times1\times8$ supercell of bcc Fe (left). The arrows illustrate the collinear spin alignments of the 16-layer Fe atoms with spin up (red) and spin down (blue). The numbers indicate the stable ferromagnetic configuration (FMC, str1) and the metastable spin-flipping configurations (SFCs, str2 ~ str12).

Generally, we select the 16-atom quasi-one-dimensional (1D) collinear magnetic configurations and ignore others (such as noncollinear, spin-wave, 2D, and 3D cases) due to the following reasons: (i) to the best of our knowledge about first-principles and phonon calculations, no successful quantitative methods exist to calculate the Helmholtz energies of other magnetic configurations except the collinear ones; (ii) the collinear case can represent the major physic phenomena (e.g., the Curie temperature, see Sec. III); (iii) it is the low energy configurations within each supercell that determine mainly the Curie transition instead of the supercell-shape (see Sec. III); (iv) the antiferromagnetic (AFM) domain wall energy or the magnetic exchange energy is depicted well in the quasi 1D case (see Sec. III); (v) less first-principles cal-

culations are needed in the 1D case since many configurations are unstable; and (vi) we believe that "simple is best" works for our model, hence, many complex magnetic issues can be resolved by using a simple collinear magnetic configurations.

C. Details of first-principles and phonon calculations

In order to use the aforementioned model in Sec. II A, Helmholtz energy of each distinguished state σ [see Eq. (1)] needs to be determined, herein, via first-principles calculations by VASP code[22] and phonon calculations by ATAT code.[23] First-principles calculations were performed by the projector augmented wave method[24] and the generalized gradient approximation[25] as implemented in the VASP code[22] using a plane-wave energy cutoff of 350 eV and a reciprocal space k-point sampling of $20\times20\times3$. The Methfessel-Paxton technique[26] was adopted to relax the $1\times1\times8$ supercell (see Fig. 1), followed by a final calculation by the tetrahedron method incorporating Blöchl correction.[27] The obtained electronic densities of state were used to determine the thermal electronic contributions to Helmholtz energy [see Eq. (1)]. Phonon calculations were performed by 64-atom supercell approach[28] (i.e., the $2\times2\times8$ supercell of bcc Fe) and the ATAT code.[23] The forces acting on atoms for each perturbed supercell were calculated by VASP[22] using the $6\times6\times2$ k-mesh and 350 eV energy cutoff. For each state shown in Fig. 1, the cutoff ranges of 4 Å were used to fit the force constants, and at least 4 volumes for each state were used to estimate the vibrational contributions to Helmholtz energy [see Eq. (1)] based on the quasiharmonic approach.[2]

III. RESULTS AND DISCUSSIONS

In order to test the effects of supercell shapes on the magnetic properties, we estimate the Curie temperature T_C of bcc Fe from the Heisenberg model in mean-field approach:[5] $T_C=2J_0/(3k_B)$ with J_0 being the magnetic exchange energy. Using the first-principles calculated static energies and the nearest-neighbor Heisenberg model, we have fitted out J_0 to be 0.148–0.1824 eV for different supercells (see Table I for details), indicating $T_C=1145-1411$ K, agreeing with the measurement [1044 K (Ref. 29)] and the previous mean-field predictions [1521 (Ref. 5) and 1335 K (Ref. 30)]. The different supercells possess the similar J_0 (see Table I), indicating the energy due to the exchange of spin-up and spin-down atoms is independent of the shape of supercell, and in turn, the energy differences between the ground state and the low energy states are nearly supercell-shape-independent. More tests of our model on different supercells using the Helmholtz free energy of state σ determined by CEM and Debye model[4] indicate that the Curie phase transition of bcc Fe depends mainly on the low energy configurations as well as their degeneracy factors [see Eq. (4)] within the supercell, similar to the importance of J_0 in mean-field model. Due to the collinear magnetic configurations used herein, the *practice* of our model using collinear cases can be considered as an improved one based on, e.g., the mean-field model and the SQS description of paramagnetic phase.

TABLE I. Predicted Curie temperatures T_C's of bcc Fe using different supercells in terms of the mean-field model (Ref. 5) $T_C=2J_0/(3k_B)$ with J_0 being the magnetic exchange energy (fitted by nearest-neighbor approach herein) and k_B the Boltzmann's constant. The measurement and other predictions of Curie temperature are also shown for comparison.

Supercell structure	Lattice vectors[a]	J_0 (eV)	T_C (K)
$1\times1\times8$ [b]	$\begin{pmatrix}1&0&0\\0&1&0\\0&0&8\end{pmatrix}$	0.1633	1263
$2\times2\times2$ [c]	$\begin{pmatrix}2&0&0\\0&2&0\\0&0&2\end{pmatrix}$	0.1744	1349
$\sqrt{8}\times\sqrt{8}\times1$ [c]	$\begin{pmatrix}2&2&0\\-2&2&0\\0&0&1\end{pmatrix}$	0.1480	1145
$\sqrt{2}\times\sqrt{2}\times4$ [c]	$\begin{pmatrix}1&1&0\\-1&1&0\\0&0&4\end{pmatrix}$	0.1824	1411
			1044[d]
			1521[e]
			1335[f]

[a]The lattice parameter of bcc Fe is set as unity 1.
[b]The predicted static energies for this supercell are accurate, see Table II.
[c]7–10 low energy structures (down-selected by CEM) are calculated by Methfessel-Paxton technique (Ref. 26) and used to fit J_0.
[d]Experiment (Ref. 29).
[e]Prediction by first-principles mean-field model (Ref. 5).
[f]Prediction by first-principles mean-field model (Ref. 30).

The resulting first-principles energy vs volume (E-V) data points of the 12 states (see Fig. 1) were fitted by the four-parameter Birch-Murnaghan equation of state.[4] The fitted E-V curves are shown in Fig. 2. The fitted properties are given in Table II, including the equilibrium volume, bulk modulus and its pressure derivative, and the relative energy with respect to str1 (the FMC structure). Evidently the FMC is the ground state at 0 K (see Fig. 2 and Table II), and the E-V curves shown in Fig. 2 will be used as the 0 K static energies in Eq. (1). Based on Fig. 2 and Table II, we find the equilibrium static energies (per supercell including 16 atoms) of SFCs relative to FMC are 0.56–0.64 eV for str2 ~ 8, 1.25–1.31 eV for str9 ~ 11, and 2.58 eV for str12. Note that the AFM domain walls within the supercell are 2 for str2 ~ 8, 4 for str9 ~ 11, and 8 for str12, indicating each AFM domain wall causes the energy increase of ~0.155 eV/atom (each AFM domain wall includes a pair of neighboring spin-up and

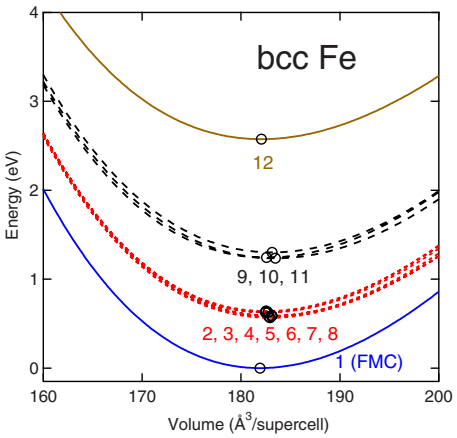

FIG. 2. (Color online) Calculated static energies at 0 K for bcc Fe in the 16-atom $1\times1\times8$ supercell. The curves are the fittings by the four-parameter Birch-Murnaghan EOS,[4] the open circles indicate the equilibrium volumes, the numbers represent the FMC and SFCs as shown in Fig. 1. The AFM domain wall energy is estimated of –0.155 eV/atom (see also Table II), where each AFM domain wall contains a pair of neighboring spin-up and spin-down atoms.

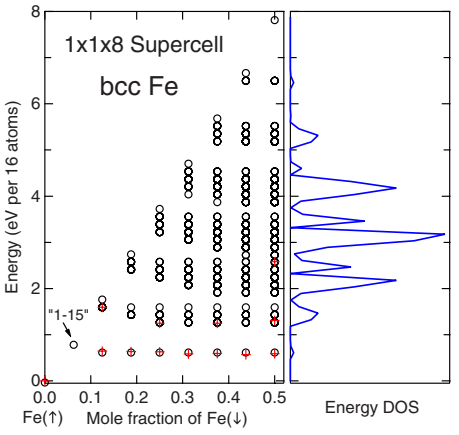

FIG. 3. (Color online) Predicted energies for all possible spin-up and spin-down configurations within the $1\times1\times8$ supercell of bcc Fe (black circles, 2250 independent structures represent the total 65 536 structures) by CEM (Refs. 19–21) with inputs from the first-principles calculated energy points (red plus symbols, see Table II). The right panel shows the energy density of state (DOS) of this supercell. Note that (i) the first and the second nearest pair ECI's are employed in CEM, (ii) the CEM predicted energies of higher Fe(↓) concentrations are not shown due to the symmetric energies, and (iii) the "1–15" structure [1 spin up (down) and 15 spin down (up) Fe atoms] is unstable based on first-principles calculations.

spin-down atoms). We note that the AFM domain wall energy (or the domain-wall-like energy in other supercells due to spin exchange) is roughly equal to the fitted magnetic exchange energy (see Table I). Based on CEM predictions, Fig. 3 shows the predicted energies and energy density of state (DOS) within the $1\times1\times8$ supercell, indicating all the low energy configurations (str2 ~ 8, see Fig. 1) have been considered herein.

Since the faultiness of Heisenberg model to capture the complete magnetic nature (see Sec. I), the present model is thus proposed to predict the magnetic properties of bcc Fe. Figure 4 shows the predicted C_P (heat capacity at constant pressure, $P=0$), where $C_P=C_V+\alpha^2BTV$ with C_V given in Eq. (5), α the volume thermal expansion coefficient, and B the isothermal bulk modulus. The predicted C_P without C_m (magnetic configurational contribution) fails to describe the

TABLE II. First-principles predicted equilibrium properties of the $1\times1\times8$ supercell for bcc Fe (see Fig. 1) via the four-parameter Birch-Murnaghan equation of state (EOS) (Ref. 4) including the equilibrium volume V_0 (Å^3 per 16 atoms), bulk modulus B_0 (GPa) and its pressure derivative (B_0'), the relative energy ΔE (eV per 16 atoms) with respect to str1 (the FMC structure), and the degeneracy factor (multiplicity) for each structure.

Structure	V_0	ΔE	B_0	B_0'	Degeneracy factor
str1 (FMC)[a]	181.96	0.000	193.0	4.61	2
str2	182.65	0.645	174.1	5.15	32
str3	182.49	0.632	178.0	4.98	32
str4	182.75	0.631	175.4	4.99	32
str5	182.89	0.585	173.5	5.09	32
str6	183.23	0.594	169.8	5.12	32
str7	183.03	0.570	171.7	5.15	32
str8	183.17	0.590	169.7	5.19	16
str9	183.26	1.249	162.7	5.13	16
str10	182.57	1.250	171.3	5.01	16
str11	183.14	1.310	168.6	4.80	8
str12	181.99	2.583	156.4	5.40	4
str13[b]	182.40	1.595	160.4	5.17	16

[a]EOS fitting for FMC is performed in the low energy and low spin magnetic region.
[b]Unstable structure due to magnetism. Its structure is similar to str9 (the 2 spin-down and 6 spin-up structure, see Fig. 1), str13 is a 1 spin-down and 7 spin-up structure. Its properties are calculated by Methfessel-Paxton technique (Ref. 26) and listed for reference only, but used to fit the ECI's for CEM.

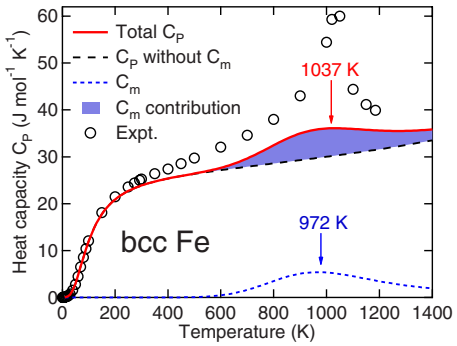

FIG. 4. (Color online) Experimental (open circles) (Ref. 6) and calculated (curves) heat capacities of bcc Fe under pressure $P=0$. The magnetic configurational entropy contributions (C_m) are obtained from the partition function due to the competition among magnetic states. A protrusion is clearly predicted with the maxima of 1037 K (from C_P) and 972 K (from C_m), pertaining to the Curie temperatures and close to the measured 1044 K (Ref. 29).

anomalous 'bump' due to phase transition at the Curie temperature [measured $T_C=1044$ K (Ref. 29)]. By including C_m, an obvious protrusion is predicted, where the maximum C_P is observed at 1037 K, pertaining to the Curie temperature. The temperature evolution of C_m, heat capacity contribution from magnetic configurational entropy, is also shown in Fig. 4, which is responsible for the anomalous C_P. We find the maximum C_m is located at 972 K, pertaining to another definition of Curie temperature owing to merely the magnetic configurational entropy. We note that the bump of the predicted C_P is still lower than the measurements.[29] The error maybe caused by (i) the missing of long-range magnetic interaction in the present model, (ii) the exclusion of unstable states, (iii) the density functional theory used for first-principles calculations, and (iv) the small size of supercell used herein (note that by a combination of the accurate energies from first principles for low energy states together with the less accurate energies from, e.g., CEM, the present model can be extended to large supercell, wherein the important states are the low energy ones). However, the anomalous C_P is predicted correctly, and the origin of anomaly is traceable to the magnetic configurational entropy due to thermodynamic fluctuations of magnetic states at evaluated temperatures.

Figure 5 shows the thermal populations of FMC and SFCs as a function of temperature under pressure $P=0$. Below ~600 K, FMC is predominant with its fraction close to unity 1. Above ~600 K, SFCs appear, resulting in the magnetic configurational entropy [see Eq. (4)] and the Schottky anomaly of C_P (see Fig. 4). At 1058 K, the population of FMC equals to the sum of SFCs (without FMC), where the cross point may also be defined as the Curie temperature since the behavior of the mixed SFCs (without FMC) is similar to the paramagnetic phase. Above 1058 K, the population of the sum of SFCs is larger than that of FMC, indicating the predominance of the paramagnetic phase. According to Eqs. (3) and (4), the temperature evolution of thermal populations of FMC and SFCs is mainly caused by the effect of magnetic configurational entropy (due to the low energy configurations).

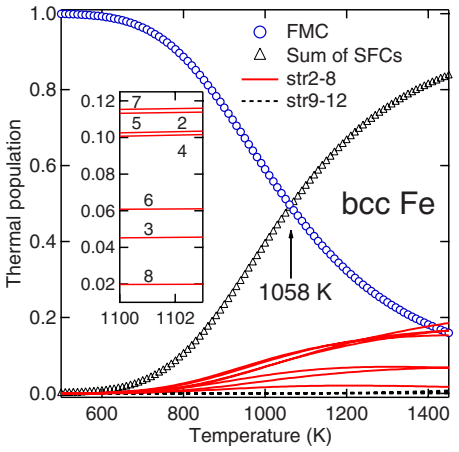

FIG. 5. (Color online) Predicted thermal populations of FMC and SFCs for bcc Fe as a function of temperature and under pressure $P=0$. The cross point at 1058 K links to another definition of Curie temperature, the numbers indicate the configurations shown in Fig. 1.

Figure 6 shows the Curie temperatures of bcc Fe as a function of pressure predicted by the methods mentioned above, i.e., the maximum of C_P, the maximum of C_m, and the equal of thermal populations between FMC and the sum of SFCs. It is worth mentioning that (i) the phase transition as shown in Fig. 6 is a second-order one due to the bump of C_P in Fig. 4 (see also Ref. 3 for the case of fcc Ce), and (ii) the illustrated pressure range (−10 to 80 GPa) is due to the E-V fittings performed in this region. The predicted Curie temperatures by the three methods form a band with the middle one from the maximum of C_P. With increasing pressure, the predicted Curie temperatures increase first ($P<4-8$ GPa) and then decrease. At pressure $P=0$, the predicted Curie temperatures of 972–1058 K (see Figs. 4 and 5) agree well with the measured 1044 K,[29] especially the one from the maximum of C_P. Note that the predictions by our model (~1000

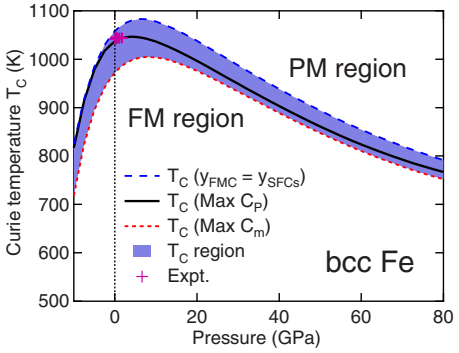

FIG. 6. (Color online) Experimental (symbols) (Ref. 29) and calculated Curie temperatures of bcc Fe as a function of pressure. The predictions are based on the maximum of C_P, the maximum of C_m, and the equal of thermal populations between FMC and the sum of SFCs ($y_{FMC}=y_{SFCs}$). The predicted T_C forms a band to separate the ferromagnetic (FM) region and the paramagnetic (PM) region and agrees with measurements, especially for the ones predicted by the maximum of C_P. The maximum T_C from predictions is located at pressure slightly larger than zero GPa.

K) is better than the ones from mean-field model (see Table I) due to the introduction of configurational entropy from partition function. The excellent predictions of Curie temperatures indicate the present model works well by using only the collinear magnetic configurations and in particular the low energy ones. We further note that the experimental values of dT_C/dP (Curie temperature with respect to pressure) were measured in the pressures of 0–2 GPa due to the restriction of phase transition between bcc and fcc phases, which are scattered and roughly constant at 1044 K.[29] We argue that the constant dT_C/dP at the pressures of 0–2 GPa is due to the maximum T_C located at $P \approx 0$ GPa. In fact, the origin of the constant dT_C/dP based on measurements is also roughly displayed in Fig. 2 and Table II: the maximum energy differences between FMC and SFCs are located around the equilibrium volumes, and the FMC possesses larger bulk modulus (~20 GPa larger) with respect to others. According to our predicted T_C in Fig. 6, the maximum T_C is located in the pressure range of 4–8 GPa, agreeing with the constant dT_C/dP from measurements. Other predictions, e.g., by mean-field theory, gave $dT_C/dP=16-18$ K/GPa,[31] while the present prediction shows $dT_C/dP=2-4$ K/GPa at lower pressure region (<4 GPa).

It is worth mentioning that the present simple model, partition function with inputs from first-principles within a simple collinear magnetic ensemble, works well not only for the present bcc Fe, but also works well for other magnetic materials, for example, we predicted the anomalous properties of heat capacity, bulk modulus, Curie/Néel temperature, and pressure-temperature phase diagram for fcc Ce,[15] iron-based superconductor $BaFe_2As_2$,[32] and other magnetic materials (unpublished works): fcc Ni, Invar alloy Fe_3Pt, and Li-ion battery material $LiFePO_4$. Therefore, we conclude that our model captures the underlying physics of magnetic materials through configurational entropy.

IV. SUMMARY

In summary, we demonstrate in bcc Fe that the magnetic thermodynamics can be resolved by an integrated partition function and collinear spin-flipping configurations (especially the low energy ones). Based completely on the inputs from first-principles phonon calculations, it is found that the Schottky anomaly of heat capacity and the occurrence of Curie temperature are due to the magnetic configurational entropy caused by the competition among the collinear magnetic states. It is worth remarking that the present model provides an alternative approach for first-principles magnetic thermodynamics besides the existing ones (e.g., Heisenberg model and Monte Carlo simulation). It is believed that the present model will be notable for magnetic thermodynamics when the long-range interaction is considered in the future. Additionally, we believe the present model could assist in decoding the mysteries in magnetic materials as well as in other materials with order-disorder phase transitions.

ACKNOWLEDGMENTS

This work was funded by the Office of Naval Research (ONR) under Contract No. N0014-07-1-0638 and the National Science Foundation (NSF) through Grant No. DMR-0510180. First-principles calculations were carried out partially on the LION clusters supported by the Materials Simulation Center and the Research Computing and Cyber infrastructure unit at the Pennsylvania State University, and partially on the resources of NERSC supported by the Office of Science of the U. S. DOE under Contract No. DE-AC02-05CH11231.

APPENDIX: THE CLUSTER EXPANSION METHOD

The cluster expansion method (CEM) (Refs. 19–21) can serve as a bridge between the first-principles calculated energies of ordered structures and the energy for any structure. In this approach the energy of a system is expanded as a rapidly convergent series of r-site multisite interaction energies, J_r, the so-called effective cluster interaction energies (ECI's),

$$E(v) = \sum_{r=0}^{r_{\max}} \xi_r J_r(v), \tag{A1}$$

where v is the volume. The sum is over all possible clusters ($r=0$ is the empty cluster). In practice the number of the maximal r-site cluster, $r_{\max}$, is limited. Note that in Eq. (A1), a set of r-site clusters may involve multiple distinguishable clusters with r sites, e.g., the two-site (pair) cluster may include the first nearest neighbor pair, the second nearest neighbor pair, etc. The ξ_r is the correlation function defined on the r-site cluster, and a set of ξ_r's can be used to characterize a structure. Note that the ξ_r's are calculated by ATAT code[23] in the present work. In matrix from, Eq. (A1) is expressed by

$$\mathbf{E} = \boldsymbol{\xi}\mathbf{J}\mathbf{V}. \tag{A2}$$

First-principles calculated energies for ordered compounds $\mathbf{E}^{\text{ord}}$ including volume effects can be fitted by e.g., the four-parameter Birch-Murnaghan EOS,[4]

$$\mathbf{E}^{\text{ord}} = \mathbf{U}^{\text{ord}}\mathbf{V}, \tag{A3}$$

where $\mathbf{U}^{\text{ord}}=[u_1\ u_2\ u_3\ u_4]$ is the matrix of the fitting parameters that describe the calculated $\mathbf{E}^{\text{ord}}$ as a function of volume, the volume matrix $\mathbf{V}=[1\ v^{-2/3}\ v^{-4/3}\ v^{-2}]'$. The superscript "ord" indicates that values are obtained for ordered compounds. $\mathbf{U}^{\text{ord}}$ and $\mathbf{V}$ are n-by-4 and 4-by-1 matrices, respectively, where n is the number of ordered compounds considered. Note that without the effect of volume, $\mathbf{E}^{\text{ord}}=\mathbf{U}^{\text{ord}}$. Using Eqs. (A2) and (A3), the ECI's can be extracted from the energies of a series of ordered compounds via the so-called Connolly-Williams-like inversion,[20]

$$\mathbf{J} = \boldsymbol{\xi}^{-1}\mathbf{U}^{\text{ord}}, \tag{A4}$$

where "−1" is the inverse or the pseudo-inverse of the

correction function matrix $\boldsymbol{\xi}$. Once we have the volume dependent ECI's by Eq. (A4), the volume dependence of **E** for any structure can be estimated by Eqs. (A2) or (A1). Using, e.g., Debye model,[4] the vibrational contribution to Helmholtz free energy for any structure can be determined and used in the present partition function approach.

*sus26@psu.edu

[1] Y. Wang, Z. K. Liu, and L. Q. Chen, Acta Mater. **52**, 2665 (2004).
[2] S. L. Shang, Y. Wang, and Z. K. Liu, Phys. Rev. B **75**, 024302 (2007).
[3] Z. K. Liu, J. Phase Equilib. Diffus. **30**, 517 (2009).
[4] S. L. Shang, Y. Wang, D. E. Kim, and Z. K. Liu, Comput. Mater. Sci. **47**, 1040 (2010).
[5] F. Körmann, A. Dick, B. Grabowski, B. Hallstedt, T. Hickel, and J. Neugebauer, Phys. Rev. B **78**, 033102 (2008).
[6] Y. S. Touloukian and C. Y. Ho, *Properties of selected ferrous alloying elements* (Hemisphere Publishing Corporation, New York, 1989).
[7] A. Zunger, S. H. Wei, L. G. Ferreira, and J. E. Bernard, Phys. Rev. Lett. **65**, 353 (1990).
[8] B. Alling, T. Marten, and I. A. Abrikosov, Nature Mater. **9**, 283 (2010).
[9] D. Hobbs, J. Hafner, and D. Spisak, Phys. Rev. B **68**, 014407 (2003).
[10] J. Wang, J. B. Neaton, H. Zheng, V. Nagarajan, S. B. Ogale, B. Liu, D. Viehland, V. Vaithyanathan, D. G. Schlom, U. V. Waghmare, N. A. Spaldin, K. M. Rabe, M. Wuttig, and R. Ramesh, Science **299**, 1719 (2003).
[11] A. K. Padhi, K. S. Nanjundaswamy, and J. B. Goodenough, J. Electrochem. Soc. **144**, 1188 (1997).
[12] N. D. Mathur, F. M. Grosche, S. R. Julian, I. R. Walker, D. M. Freye, R. K. W. Haselwimmer, and G. G. Lonzarich, Nature (London) **394**, 39 (1998).
[13] C. K. Xu and S. Sachdev, Nat. Phys. **4**, 898 (2008).
[14] J. Zaanen, Nature (London) **457**, 546 (2009).
[15] Y. Wang, L. G. Hector, H. Zhang, S. L. Shang, L. Q. Chen, and Z. K. Liu, Phys. Rev. B **78**, 104113 (2008); J. Phys.: Condens. Matter **21**, 326003 (2009).
[16] P. M. Chaikin and G. Beni, Phys. Rev. B **13**, 647 (1976).
[17] M. J. van Setten, M. A. Uijttewaal, G. A. de Wijs, and R. A. de Groot, J. Am. Chem. Soc. **129**, 2458 (2007).
[18] M. Widom and M. Mihalkovic, Phys. Rev. B **77**, 064113 (2008).
[19] A. van de Walle and G. Ceder, J. Phase Equilibria **23**, 348 (2002).
[20] J. W. D. Connolly and A. R. Williams, Phys. Rev. B **27**, 5169 (1983).
[21] S. Shang and A. Bottger, Acta Mater. **53**, 255 (2005).
[22] G. Kresse and J. Furthmuller, Phys. Rev. B **54**, 11169 (1996).
[23] A. van de Walle, Calphad **33**, 266 (2009).
[24] G. Kresse and D. Joubert, Phys. Rev. B **59**, 1758 (1999).
[25] J. P. Perdew, K. Burke, and M. Ernzerhof, Phys. Rev. Lett. **77**, 3865 (1996).
[26] M. Methfessel and A. T. Paxton, Phys. Rev. B **40**, 3616 (1989).
[27] P. E. Blöchl, O. Jepsen, and O. K. Andersen, Phys. Rev. B **49**, 16223 (1994).
[28] A. van de Walle and G. Ceder, Rev. Mod. Phys. **74**, 11 (2002).
[29] J. M. Leger, C. Loriers-Susse, and B. Vodar, Phys. Rev. B **6**, 4250 (1972).
[30] M. Pajda, J. Kudrnovsky, I. Turek, V. Drchal, and P. Bruno, Phys. Rev. B **64**, 174402 (2001).
[31] S. Morán, C. Ederer, and M. Fahnle, Phys. Rev. B **67**, 012407 (2003).
[32] Y. Wang, S. L. Shang, L. Q. Chen, and Z. K. Liu, Int. J. Quantum Chem. (to be published).